John von Neumann Institute for Computing

Parallel Simulation of Turbulent Magneto-hydrodynamic Flows

Axelle Viré, Dmitry Krasnov, Bernard Knaepen, Thomas Boeck

published in

Parallel Computing: Architectures, Algorithms and Applications ,
C. Bischof, M. Bücker, P. Gibbon, G.R. Joubert, T. Lippert, B. Mohr, F. Peters (Eds.),
John von Neumann Institute for Computing, Jülich,
NIC Series, Vol. **38**, ISBN 978-3-9810843-4-4, pp. 483-490, 2007.
Reprinted in: Advances in Parallel Computing, Volume **15**,
ISSN 0927-5452, ISBN 978-1-58603-796-3 (IOS Press), 2008.

http://www.fz-juelich.de/nic-series/volume38

Parallel Simulation of Turbulent Magneto-hydrodynamic Flows

Axelle Viré[2], Dmitry Krasnov[1], Bernard Knaepen[2], and Thomas Boeck[1]

[1] Fakultät für Maschinenbau, Technische Universität Ilmenau
P.O. Box 100565, 98684 Ilmenau, Germany
E-mail: {thomas.boeck, dmitry.krasnov}@tu-ilmenau.de

[2] Université Libre de Bruxelles, Service de Physique Théorique et Mathématique
Campus Plaine - CP231, Boulevard du Triomphe, 1050 Brussels, Belgium
E-mail: {bknaepen, avire}@ulb.ac.be

We compare the performances of a pseudospectral and a finite-volume method for the simulation of magnetohydrodynamic flows in a plane channel. Both Direct Numerical Simulations (DNS) and Large-Eddy Simulations (LES) are performed. The LES model implementation is validated for non-conductive flows. The application of the LES model in the case of flows subjected to low intensity magnetic fields is shown to be successful.

1 Introduction

Turbulent magnetohydrodynamic (MHD) flows at low magnetic Reynolds number, i.e. flows of electrically conducting liquids in the presence of an external magnetic field, occur in a variety of metallurgical processes. MHD flows are affected by the Lorentz force arising from the induced electric currents in the liquid. Important examples are the electromagnetic braking of molten steel in continuous casting or the electromagnetic stirring of melts[1]. By comparison with ordinary fluid flows, the experimental investigation of MHD flows is complicated by the opacity and corrosiveness of liquid metals. Experiments typically provide very limited information on the flow structures and statistics. For this reason, the accurate prediction of such flows by numerical simulations is of particular interest.

The purpose of the present study is to investigate the MHD channel flow by performing Large-Eddy Simulations (LES) and to compare two numerical approaches, the pseudospectral method and the finite-volume one, in terms of parallel computing performances. The attention is restricted to the case of a plane channel with a wall-normal magnetic field and electrically insulating boundaries. Such a geometry is known as the Hartmann flow. As illustrated in Fig. 1 (from Boeck *et al.*[2]), its remarkable features are a suppression of turbulent fluctuations (i.e. flat profile) in the middle of the channel and two boundary layers at the walls, where the current loops close. Moreover, the boundary layers become thinner as the imposed magnetic field intensity increases.

As a consequence, compared to the hydrodynamic case, the presence of the magnetic field imposes the use of a finer mesh, close to the walls, leading to higher computational costs. Hence, LES is likely to prove very useful to simulate MHD flows in that it reduces the global number of grid points. However, considerable computational ressources are still needed when more flexible codes are used. Direct Numerical Simulations (DNS) of MHD channel flows have been investigated intensively by Boeck *et al.*[2]. Their results, obtained with a pseudospectral code, are used here as a benchmark for the LES simulations of MHD

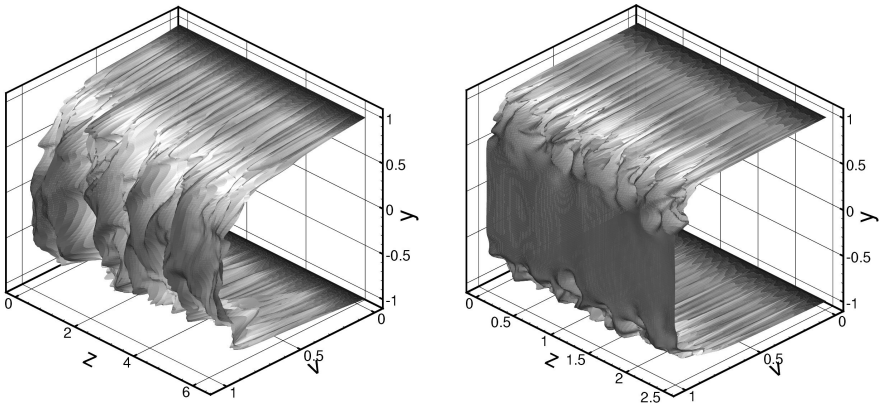

Figure 1. Effect of the wall-normal magnetic field on a turbulent channel flow. Snapshots of the streamwise velocity component in a plane $x = const$ for a non-magnetic flow at a Reynolds number $Re_c = U_c\delta/\nu = 3300$, based on the mean centreline velocity U_c and the channel half-width δ (left); and for a turbulent Hartmann flow at $R = 500$ and $Ha = 30$ (right) (for additional definitions see Section 2.1).

flows.

2 Mathematical Model

2.1 Basic MHD Equations

When an electrically conducting fluid is set in motion in the presence of an external magnetic field, the flow is affected by the Lorentz force. This has globally dissipative and anisotropic effects and, therefore, it modifies the turbulence structures present in the flow. The relative importance of the nonlinear and the diffusion terms in the magnetic induction equation is quantified by the magnetic Reynolds number Re_m. In the limit of low Re_m, the so-called *quasi-static approximation*, the effect of the magnetic field is taken into account through an extra damping term[3]. This leads to the incompressible Navier-Stokes Eq. (2.1), in which ρ, μ, σ are the fluid density, molecular viscosity and electrical conductivity, respectively; and u, P, B are the velocity, pressure and external magnetic field. The induced electric current j is given by Ohm's law, $\mathbf{j} = \sigma(-\nabla\Phi + \mathbf{u} \times \mathbf{B})$, assuming that the electric field is the gradient of the electric potential $\Phi = \nabla \cdot (\mathbf{u} \times \mathbf{B})$. In Eq. (2.1), ϵ_{ijk} represents the permutation symbol.

$$\rho\partial_t u_i + \rho\partial_j(u_i u_j) = -\partial_i P + \mu\partial_j\partial_j u_i + \sigma\epsilon_{ijk} j_j B_k \qquad i,j,k = 1,...,3 \tag{2.1}$$

Notice that we use the summation convention, and that the incompressibility requires $\partial_j u_j = 0$. By introducing the friction velocity u_τ and the characteristic length δ, Eq. (2.1) can be non-dimensionalized, leading to

$$\partial_t u_i^+ + \partial_j(u_i^+ u_j^+) = -\partial_i p^+ + \frac{1}{Re_\tau}\partial_j\partial_j u_i^+ + N\epsilon_{ijk} j_j^+ B_k^+ \qquad i,j,k = 1,...,3. \tag{2.2}$$

In Eq. (2.2), $p = P/\rho$ and $\nu = \mu/\rho$ are the kinematic pressure and viscosity, respectively. In addition, non-dimensional parameters are introduced: the friction Reynolds

number $Re_\tau = u_\tau \delta/\nu$ and the interaction parameter $N = \sigma B^2 \delta/\rho u_\tau$. Additional non-dimensional parameters are often used to describe MHD flows: the Hartmann number $Ha = B\delta\sqrt{\sigma/\rho\nu}$ which quantifies the intensity of the magnetic field, and the Reynolds number $R = U_0 d/\nu$ based on the laminar centreline velocity U_0 and on the Hartmann layer thickness $d = B^{-1}\sqrt{\rho\nu/\sigma}$. The superscript $+$, which denotes non-dimensional quantities, will be omitted in the rest of this paper.

2.2 Filtering and Subgrid-Scale Model

LES equations are obtained by spatially filtering Eq. (2.2). In Eq. (2.3), the overbar denotes the "grid-filter", whose kernel is G, and which eliminates the small scale part of the discrete velocity field. The filtered velocity $\overline{u}_i$ is defined by Eq. (2.4).

$$\partial_t \overline{u}_i + \partial_j(\overline{u_i u_j}) = -\partial_i \overline{p} + \frac{1}{Re_\tau}\partial_j\partial_j \overline{u}_i + N\overline{\epsilon_{ijk} j_j B_k} \tag{2.3}$$

$$\overline{u}_i(\mathbf{x}) = \int G(\mathbf{x},\mathbf{y}) u_i(\mathbf{y}) d\mathbf{y} \tag{2.4}$$

Filtering of the incompressibility condition leads to $\partial_j \overline{u}_j = 0$. Because we are using the quasi-static approximation, the only non-linear term in Eq. (2.3) is the convective term. Therefore, writing Eq. (2.3) as:

$$\partial_t \overline{u}_i + \partial_j(\overline{u}_i \overline{u}_j) = -\partial_i \overline{p} + \frac{1}{Re_\tau}\partial_j\partial_j \overline{u}_i + N\overline{\epsilon_{ijk} j_j B_k} - \partial_j \overline{\tau}_{ij}, \tag{2.5}$$

we see that only the subgrid-scale stress tensor $\overline{\tau}_{ij} = \overline{u_i u_j} - \overline{u}_i \overline{u}_j$ has to be modelled in order to close the equation in terms of the filtered velocity. The most commonly used model is the Smagorinsky model,

$$\overline{\tau}_{ij} = -2\nu_e \overline{S}_{ij} + \frac{1}{3}\delta_{ij}\overline{\tau}_{kk}, \tag{2.6}$$

in which δ_{ij} is the Kronecker symbol, $\nu_e = C_s \overline{\Delta}^2 |\overline{S}|$ is the eddy viscosity, C_s is the Smagorinsky constant, $\overline{\Delta}$ is the grid-filter width, and $|\overline{S}| = (2\overline{S}_{ij}\overline{S}_{ij})^{1/2}$ is the magnitude of the large-scale strain-rate tensor $\overline{S}_{ij} = 1/2(\partial_j \overline{u}_i + \partial_i \overline{u}_j)$. However, this model uses a single constant C_s and turns out to be inefficient in several cases: modelling of inhomogeneous turbulence, backscatter, etc. For this reason, a dynamic procedure has been developed[4], which aims to overcome the previously mentioned drawbacks by dynamically computing C_s. This is achieved by introducing a second, coarser spatial filter, the "test-filter", denoted by $\widehat{...}$, whose width is $\widehat{\overline{\Delta}}$. The LES equation is re-written as

$$\partial_t \widehat{\overline{u}}_i + \partial_j(\widehat{\overline{u}}_i \widehat{\overline{u}}_j) = -\partial_i \widehat{\overline{p}} + \frac{1}{Re_\tau}\partial_j\partial_j \widehat{\overline{u}}_i + N\widehat{\overline{\epsilon_{ijk} j_j B_k}} - \partial_j \widehat{T}_{ij}, \tag{2.7}$$

in which $\widehat{T}_{ij} = \widehat{\overline{\tau}}_{ij} - \widehat{\overline{u}}_i \widehat{\overline{u}}_j + \widehat{\overline{u_i u_j}}$. Assuming that both levels of filtering use the same C_s (self-similarity hypothesis), which means $\widehat{C}_s \approx C_s$, the Smagorinsky parameter is expressed by

$$C_s = \frac{1}{2}\frac{\langle L_{ij}\widehat{\overline{S}}_{ij}\rangle_{xz}}{\langle M_{ij}\widehat{\overline{S}}_{ij}\rangle_{xz}}, \tag{2.8}$$

where

$$L_{ij} = \widehat{T}_{ij} - \widehat{\overline{\tau}}_{ij}, \quad M_{ij} = \overline{\Delta}^2 | \widehat{\overline{S} \mid \overline{S}_{ij}} - \widehat{\overline{\Delta}}^2 \mid \widehat{\overline{S}} \mid \widehat{\overline{S}}_{ij}. \tag{2.9}$$

Because of the flow homogeneity in the wall-parallel directions x, z of the channel, a single value of the Smagorinsky parameter can be assumed in each $y = const.$-plane[5]. Thus, in Eq. (2.8), $\langle ... \rangle_{xz}$ denotes an averaging procedure in these planes. All LES results presented in this paper are obtained with the dynamic Smagorinsky model (DSM) by applying local grid and test filters in planes parallel to the channel walls, whereas the averaging procedure in the computation of C_s is performed globally in these planes. The test to grid filter ratio $\widehat{\overline{\Delta}}/\overline{\Delta}$ is set to 2.

3 Numerical Codes for Wall-Bounded Flows

3.1 Pseudospectral Method (PSM)

The pseudospectral code used in this study is described in Boeck *et al.*[2]. The method applies a Fourier expansion in horizontal directions where periodic boundary conditions are imposed, and a Chebyshev polynomial expansion in the vertical direction between insulating walls (no-slip conditions). The time-stepping scheme uses three time levels for the approximation of the time derivative and is second-order accurate. The computation of the subgrid-scale (SGS) term can be disabled, so that the flow solver can be used for both DNS and LES calculations. The parallelization of the pseudospectral algorithm is accomplished by a domain decomposition with respect to the x or z direction. Only the Fourier transforms will then require inter-process communication. In our implementation, the transform proceeds as a successive application of one-dimensional transforms with respect to x, z and y. The transform for the divided direction is avoided by a transposition of the data array containing the expansion coefficients. The interprocess communication utilizes the Message Passing Interface (MPI) library.

3.2 Finite-Volume Method (FVM)

The numerical solution is based on the discretization in finite volumes of the integral form of the Navier-Stokes equations. Compared to spectral codes, the finite-volume method has the advantage that it can deal with very complex geometries often encountered in industrial applications. Depending on the grid arrangement, two formulations can be defined: the first is based on a staggered mesh, in which the pressure is computed at the cell centre, whereas the velocity components are calculated at the cell faces; the second uses a collocated mesh, in which both pressure and velocity components are computed at the cell centre. In both cases, interpolations are necessary to obtain variables at the faces from the grid ones. For simulations in complex geometries, the second method is favoured over the first one due to its simpler form in curvilinear coordinates[7]. However, non-staggered grids require special care to handle the well-known velocity/pressure decoupling. In the present code, this is done by introducing an implicit smoothing of the pressure by interpolation[8]. For this reason, a collocated-mesh scheme introduces a non-conservation error, unlike the staggered-mesh formulation[7]. The present simulations are performed with the CDP code developed at the Center for Turbulence Research (NASA Ames/Stanford University)[8,9].

A semi-implicit (Adams–Bashforth/Crank–Nicholson) time-splitting method is chosen for time advancement[10] while a collocated formulation is adopted for the spatial discretization. The parallelization is based on the MPI standard. The solver has been extended to deal with LES of MHD flows.

4 Results

4.1 Code Validation

Implementations are validated by comparing hydrodynamic channel flow simulations with those of Kim *et al.*[11]. A constant mass flow rate is imposed so that $Re_b = 2U_b\delta/\nu = 5600$, where Re_b is the bulk Reynolds number and $U_b = \int_{-\delta}^{\delta} U(y)dy/2\delta$ is the bulk velocity (δ is chosen as the channel half-width). This results in $Re_\tau \approx 180$, where u_τ is defined through the wall shear stress ρu_τ^2. Table 1 shows the three test cases considered. In both codes, periodic boundary conditions are applied in the homogeneous directions (i.e. streamwise and spanwise) and the mesh spacing is stretched in the wall-normal direction according to the distribution of Chebyshev collocation points. The domain size is $(4\pi\delta) \times (2\delta) \times (2\pi\delta)$ in the streamwise, wall-normal and spanwise directions, respectively. Results obtained

Case ID	Mesh resolution	Subgrid-scale model
udns64	$64 \times 64 \times 64$	No
les64	$64\times 64 \times 64$	DSM
udns128	$128 \times 128 \times 128$	No

Table 1. Hydrodynamic channel flow simulations. The acronym udns refers to an unresolved direct numerical simulation, i.e. without LES model and insufficient grid resolution.

from both codes are in good agreement with the literature ones. For the $udns128$ case, the friction Reynolds number is equal to 177.98 using the FVM and to 183.16 with the PSM. However, the PSM approach is more accurate than the FVM for coarser resolutions. In fact, the $les64$ case gives $Re_\tau \approx 167.12$ using the FVM and $Re_\tau \approx 178.32$ using the PSM. Hence, considering that a difference in Re_τ of approximately one percent compared to the DNS value is fairly good, the accuracy of the PSM is satisfactory at coarse resolutions if a LES model is used. The inaccuracy of the finite-volume simulation is due to a higher numerical dissipation and a more detailed analysis of the different contributions to the total dissipation has to be performed.

4.2 Parallel Performance Benchmarks

The aim of this part is to compare the computational cost of the PSM with that of the FVM, with and without LES model. All the simulations are run on our cluster made of four 3.0 GHz, 8-core Intel Xeon-based Mac Pro nodes. The nodes are connected through a standard gigabit Ethernet network. Internal communications utilize the local bus and shared memory.

Case	Number of CPU's	Run time per 10000 iterations [hours]	% CPU
udns64	1 (1 node)	1.8	100
udns64	2 (1 node)	1.00	100
udns64	4 (1 node)	0.71	92
udns64	8 (1 node)	0.65	46
les64	1 (1 node)	5.53	100
les64	2 (1 node)	3.32	93
les64	4 (1 node)	2.86	85
les64	8 (1 node)	2.57	43
udns128	1 (1 node)	16.57	100
udns128	2 (1 node)	9.74	95
udns128	4 (1 node)	6.76	90
udns128	8 (1 node)	6.25	46

Table 2. Performance study for the PSM. % CPU refers to the utilization of individual CPUs as shown by the UNIX *top* command.

Table 2 illustrates that, using our cluster, the cost of the LES implementation in the spectral code is about three times the total run time without model, for the same mesh resolution. An evaluation of the time spent on inter-process communication is also performed by comparing performances using 8 cores located in the same node or on two different nodes. The main results obtained with the finite-volume code are given in Table 3.

The advantage of the FVM is that the DSM only represents 10.7% of the total run time which is much less than for the PSM. However, this comes at the cost of accuracy which is higher in the PSM (see Section 4.1). In fact, the FVM becomes competitive at very high mesh resolutions or in the case of complex geometries, which cannot be studied with a spectral approach. Moreover, the performance of the gigabit Ethernet connection is evaluated by comparing the run time of the $udns64$ case on 8 CPU's in one node with that in two nodes. Using the FVM, 19.4% of run time is saved when the 8 CPU's are in the same node. Finally, as the run time of the $udns64$ simulation on 4 CPU's is identical

Case	Number of CPU's	Run time per 10000 iterations [hours]	% CPU
udns64	1 (1 node)	22.5	100
udns64	2 (1 node)	14.58	100
udns64	4 (1 node)	8.61	100
udns64	8 (1 node)	6.94	100
udns64	8 (2 nodes)	8.61	85
les64	8 (1 node)	7.77	100
udns128	16 (2 nodes)	52.77	82

Table 3. Performance study for the FVM.

Case	R	Ha	Mesh resolution in DNS^2	Mesh resolution in LES
case1	700	20	$256 \times 256 \times 256$	$64 \times 64 \times 64$
case2	700	30	$512 \times 256 \times 512$	$128 \times 128 \times 128$

Table 4. Results for turbulent Hartmann flows from pseudospectral code.

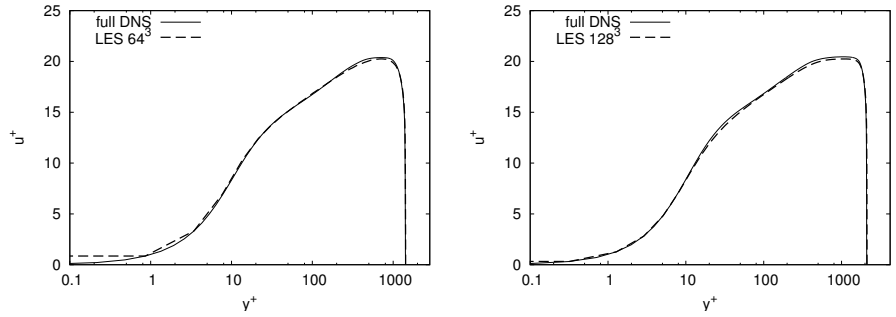

Figure 2. DNS vs. LES for turbulent Hartmann flows, mean velocity profiles in wall units for case1 (left) and case2 (right). DNS and LES resolutions are correspondingly 256^3 vs. 64^3 for the first case and $512^2 \times 256$ vs. 128^3 for the second one.

to that on 8 CPU's but on two nodes, the main bottleneck of the cluster is the time lost in network connections.

4.3 Large-Eddy Simulations of Hartmann Flow

In this section, the performance of the DSM is analysed in the case of the turbulent Hartmann flow. The two cases considered are presented in Table 4 and results are compared with the database made by Boeck *et al.*[2]. Using the DSM in LES runs, $case1$ and $case2$ yield to $Re_\tau = 707.4$ and $Re_\tau = 1064.3$, respectively, compared with $Re_\tau = 708.6$ and $Re_\tau = 1047.3$ for the corresponding DNS values. The performance of the SGS model is also illustrated by Fig. 2 which shows profiles of the mean velocity in wall units (i.e. non-dimensionalized by u_τ and δ). The comparison clearly indicates that LES mean velocities are in good agreement with the DNS ones. As a result, the standard DSM proves to be successful in modelling MHD flows using numerical grids about four times coarser than the DNS ones.

5 Conclusions

This work aims to evaluate the performance of the PSM and FVM, in terms of computational cost and accuracy. It reveals that, if the same mesh resolution is used in both approaches, the flexibility of the finite-volume code comes at the cost of accuracy. In other words, the FVM requires higher mesh resolutions than the spectral one to obtain the same

level of accuracy. For this reason, LES is likely to prove very useful to decrease the resolution requirements. In that perspective, this study shows that the advantage of the FVM is that the additional cost introduced by the LES model is not significant compared with the total run time. In particular, for a standard LES test case, Section 4.2 shows that the cost of the LES model is about 300% using the spectral code compared with 10% with the finite-volume method. As a consequence, the FVM becomes competitive at very high resolution simulations. However, because of the loss of accuracy in the finite-volume approach, attention has to be paid to avoid the numerical dissipation from becoming higher than the LES contribution. In this context, further work needs to be done to evaluate the balance between numerical and subgrid-scale dissipations.

Acknowledgements

TB and DK acknowledge financial support from the DFG in the framework of the Emmy-Noether program (grant Bo1668/2-2) and computer resources provided by the NIC. AV is supported by a F.R.I.A. fellowship. BK acknowledges financial support through the EU-RYI (European Young Investigator) Award "Modelling and simulation of turbulent conductive flows in the limit of low magnetic Reynolds number".

References

1. P. A. Davidson, *Magnetohydrodynamics in materials processing*, Annu. Rev. Fluid Mech., **31**, 273–300, (1999).
2. T. Boeck, D. Krasnov and E. Zienicke, *Numerical study of turbulent magnetohydrodynamic channel flow*, J. Fluid Mech., **572**, 179–188, (2007).
3. B. Knaepen and P. Moin, *Large-eddy simulation of conductive flows at low magnetic Reynolds number*, Phys. Fluids, **16**, 1255–1261, (2004).
4. M. Germano, U. Piomelli, P. Moin and W. H. Cabot, *A dynamic subgrid-scale eddy viscosity model*, Phys. Fluids, **A 3**, 1760–1765, (1991).
5. D. K. Lilly, *A proposed modification of the Germano subgrid-scale closure method*, Phys. Fluids, **A 4**, 633–635, (1992).
6. T. Boeck, D. Krasnov, M. Rossi, O. Zikanov and B. Knaepen, *Transition to turbulence in MHD channel flow with spanwise magnetic field*, in: Proc. Summer Programm 2006, Center for Turbulence Research, Stanford University, (2006).
7. F. N. Felten and T. S. Lund, *Kinetic energy conservation issues associated with the collocated mesh scheme for incompressible flow*, J. Comp. Phys., **215**, 465–484, (2006).
8. F. Ham and G. Iaccarino, *Energy conservation in collocated discretization schemes on unstructured meshes*, Annual Research Briefs, Center for Turbulence Research, Stanford University, 3–14, (2004).
9. K. Mahesh, G. Constantinescu and P. Moin, *A numerical method for large-eddy simulation in complex geometries*, J. Comp. Phys., **197**, 215–240, (2004).
10. J. Kim and P. Moin, *Application of a fractional-step method to incompressible Navier–Stokes equations*, J. Comp. Phys., **59**, 308–323, (1985).
11. J. Kim, P. Moin and R. Moser, *Turbulence statistics in fully developed channel flow at low Reynolds number*, J. Fluid Mech., **177**, 133–166, (1987).